Development of a Damage Quantification Model for Composite Skin-Stiffener Structures

R. Loendersloot, T.H. Ooijevaar, A. de Boer
Structural Dynamics & Acoustics, Faculty of Engineering Technology, University of Twente (UT), Enschede, The Netherlands

R. Akkerman
Production Technology, Faculty of Engineering Technology, University of Twente (UT), Enschede, The Netherlands

ABSTRACT: The development of a model-based approach for a damage severity assessment applied on a complex composite skin structure with stiffeners is presented in this paper. Earlier investigations on composite structures with stiffeners revealed that a vibration based structural health monitoring approach, employing the *Modal Strain Energy Damage Index* (MSE-DI) algorithm can detect and localise delaminations. The next step, performed in the presented part of the research, is to assess the severity of the damage. It is shown that combining results from a frequency based analysis and from a modal strain energy based analysis can enhance the quantification of the severity estimation. This conclusion was drawn by analysing the effect of small masses that were added at a specific location in to mimic a damage, but maintain reversibility of the damage. The use of a numerical model to create a virtual test space was found to be valuable for the interpretation of experimental data.

1 INTRODUCTION

A substantial amount of research effort is spent over the past years on Structural Health Monitoring (SHM) for civil, offshore, oil and aerospace applications (Fan & Qiao 2011, Montalvão et al. 2006). The latter is a still relatively new area of research. This is due to the complexity of the components and the high demands on safety and reliability of the SHM-system.

A wide range of technologies, comprising structural vibration and propagating wave technologies is employed for health monitoring purposes. The first method provides data that is relatively easy to interpret. More complex structure can be analysed with this method and a relatively large area can be explored at once. The frequency range, and hence the resolution, is however limited. As a consequence, only relatively large damages such as delaminations can be detected and localised (Fritzen & Kraemer 2009). Typical applications are found in civil structures such as bridges (Farrar & Jauregui 1998a, b, Stubbs et al. 2000, Lee & Yun 2006, Li et al. 2007).

Wave propagating technologies, employing higher frequencies, are considered to be more powerful, as they are capable of detecting small damages such as cracks (Su et al. 2006, Raghavan & Cesnik 2007, Ihn & Chang 2008, Schulte & Fritzen 2010). An increasing interest can be observed for wave propagation technologies, both in experimental (Ihn & Chang 2008, Staszewski et al. 2009) as well as in numerical research (Kudela et al 2007, 2008, Kudela & Ostachowicz 2009, Lee & Staszewski 2003a, b). The downside is the more complex interpretation of the data, in particular in case it concerns non-flat structures.

The selection of the best technology for an SHM-system is therefore often all but straightforward and finally a matter of compromises. Successful damage detection and localisation algorithms have been developed based on both structural vibration and wave propagation technologies. Here, the structural vibration approach is selected, because the structure (panel with

stringers) and the material (multi-layered composite) are relatively complex and the initial goal is to identify relatively large damages such as delamination (hence: no microcracks).

A distinction can be made between models that use frequency and modal parameters directly (direct modal based models), such as the natural frequencies and MAC values (Salawu 1997), and models that use derived modal parameters (extended modal based models), such as the modal flexibility (Alvandi & Cremona 2006) and modal strain energy (Stubbs et al. 1995, Alvandi & Cremona 2006) based algorithms. The first are generally only capable of detecting damage, which is referred to as level 1 damage identification (Fritzen & Kraemer 2009). The other methods listed are also capable of localisation of the damage, referred to as level 2 damage identification (Fritzen & Kraemer 2009).

A limitation of all technologies is the ability to estimate the severity of the damage accurately. However, a robust and reliable SHM-system depends on a damage severity assessment. Hence an evolution from level 2 to level 3 (diagnostic, see Fritzen & Kraemer 2009) damage identification can be considered as a crucial step forward to realise SHM-applications. Damage severity indexes related to the modal strain energy are introduced (Stubbs et al. 1995, Choi et al. 2006), but lack confidence. Earlier, it was suggested by others that changes in the modal parameters can be used for a damage severity assessment, despite their damage localisation incapabilities (Ndambi et al. 2002). Combination of technologies is therefore a potentially strong alternative. This concept is explored here for a composite skin-stiffener structure, as frequently used in the aerospace industry.

2 COMPOSITE SKIN-STIFFENER STRUCTURES

This research concentrates on carbon fibre reinforced thermoplastic (PEKK) skins with multiple stiffeners. A skin-stiffener structure is vulnerable for delamination damage at the skin-stiffener interfaces. Experimental and numerical studies were performed preceding this research on two structures: A slender beam (1m long) with a single stiffener (Loendersloot et al 2009, Ooijveaar et al. 2010a) and a small plate (length x width: 400mm × 282mm) with three stiffeners over the length (Ooijevaar et al. 2010b, Loendersloot et al. 2010). These studies showed that delamination damage can be detected and localised by vibration based technologies combined with the *Modal Strain Energy Damage Index* (MSE-DI) algorithm (first introduced by Stubbs et al. 1995). The experiments were performed using a shaker induced random force excitation and a laser vibro system measuring system. The numerical models were implemented in a commercial Finite Element package.

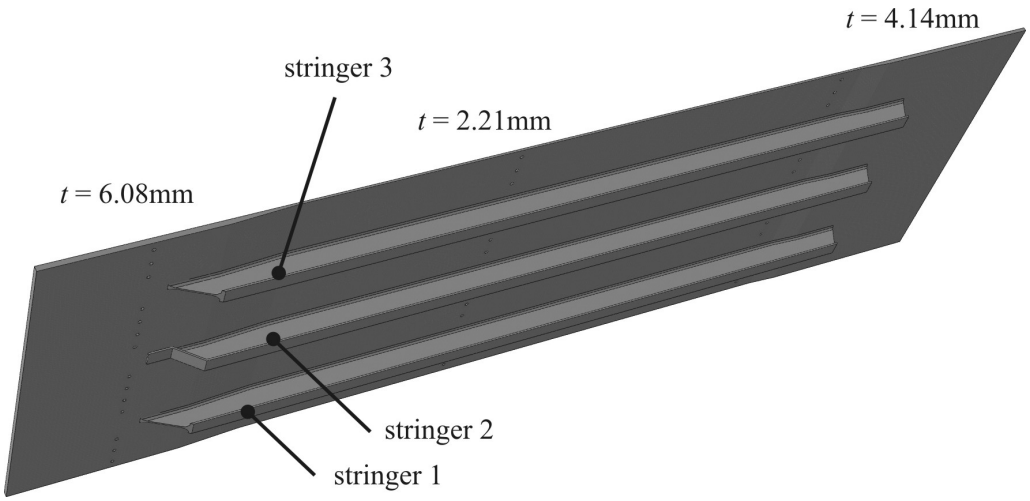

Figure 1. Three dimensional view of the panel with three stringers (stiffeners).

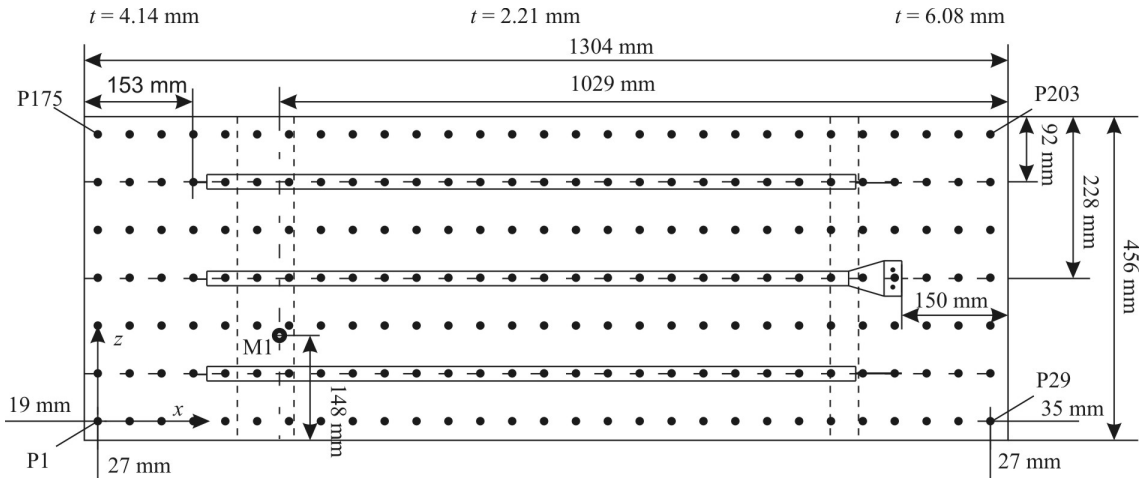

Figure 2. Bottom view of the panel, indicating the dimensions and locations of measuring points (dots) and location of the added mass (M1). The dashed lines indicate the edges of the transition zones between the sections with different thicknesses.

A larger plate (length × width: 1304mm × 456mm) also with three stiffeners over the length and with a non-uniform thickness distribution was manufactured (Fig. 1), as the smaller plate appeared to be unsuitable for damage severity analysis. The plate consists of a 16-layer, quasi-isotropic midsection and 44-layer and 30-layer end sections. The stiffeners are made of a 15-layer quasi-isotropic stack (middle layer is a 90° layer, with respect to the length of the plate). The geometry of the plate is shown in Figure 2. The material properties of the PEKK based UD composite are listed in Table 1.

Table 1. Material properties for uni-directional carbon reinforced PEKK.

E_1 [GPa]	E_2=E_3 [GPa]	ν_{12} [-]	ν_{13}=ν_{23} [-]	G_{12}=G_{13}=G_{23} [GPa]	ρ [kg·m^{-2}]
134	9.65	0.3	0.45	5.3	1590

Earlier results (Loendersloot et al. 2010) pointed out that an impact damage is relatively uncontrolable. This hampers the validation of numerical models, in particular concerning the severity of the damage. It was shown that localisation is relatively straight forward, but the relation with the shape of the delamination and the damage index analysed is far from trivial. Therefore, a controlled change of the structure is analysed, prior to analysing an actual damage case. The main condition for the controlled change is that the effect has to be reversible. This was achieved by adding small masses to the structure (see Figure 2, for the exact location M1 where the mass was added). Dynamic measurements, using a laser-vibrometer, were performed on the structure with and without an added mass weighing 42 grams (~1.1% of the total weight). The measurements are discussed in Ooijevaar et al. (2011).

A model-based approach is opted, based on the previous experiences with both experimental work and numerical models. Combining these improves the interpretation of the data measured in an actual application. The numerical model is implemented in Abaqus®. Shell elements are employed, combined with the composite lay-up option implemented in Abaqus®, hence allowing to specify each individual layer of UD material separately, respecting its orientation relative to the global coordinate system. The transition zones from the thicker end sections to the 16-layer mid section are modelled according to the lay-up specifications provided by Fokker Aerostructures.

3 DAMAGE SEVERITY ASSESSMENT

An extended modal technique was used in the previous researches (Loendersloot et al. 2009, 2010, Ooijevaar et al. 2010a, b); more specifically, the *modal strain energy damage index* (MSE-DI) algorithm, as first introduced by Stubbs et al. (1995), was implemented. The motivation to use an extended modal based damage identification algorithm, is twofold: Firstly, these

extended algorithms tend to be more sensitive to damage, enhancing the detectability compared to direct modal based algorithms using dynamic properties, such as shifts in the natural frequencies (Salawu 1997, Grouve et al. 2008). Secondly, extended modal based algorithms allow for damage localisation, hence allowing the step from level 1 damage identification to level 2. There have been a number of researches to assess the severity of the damage (level 3), using the extended modal based identification methods. So far, the success of these severity estimations is not satisfactory (Choi et al. 2006, Li et al 2006).

3.1 *Direct modal based identification methods*

Dynamic properties of a structure such as the natural frequencies and the mode shapes can usually be determined directly from the measurements. The response of a damaged structure will differ in the sense that the natural frequencies will shift and the mode shapes will be changed subtly (Salawu 1997, Grouve et al. 2008). Different techniques are available to determine the natural frequencies and mode shapes experimentally and numerically. The main difference between the experimental and numerical techniques is that a specific natural frequency analysis can be performed numerically, by means of solving the generalised eigen value problem of the numerical model (for example using a Lanczos solver), whereas the natural frequencies are determined indirectly from a response analysis in case of an experimental analysis. Both *Experimental Modal Analysis* (EMA) and *Operational Modal Analysis* (OMA) can be employed (Schwarz & Richardson 1999) to extract the modal parameters.

The change in the mode shapes can be determined based on the *Modal Assurance Criterion* (MAC). This criterion is a mathematical comparison between to vectors φ_1 and φ_2 defined as

$$MAC = \frac{\left(\varphi_1^T \varphi_2\right)^2}{\left(\varphi_1^T \varphi_1\right)\left(\varphi_2^T \varphi_2\right)} \tag{1}$$

The MAC value is mostly used to match experimental and numerical modes. As a result, the numerical vector φ is limited to the number of points measured, although the number of nodes in the numerical model can be significantly higher.

A variant of the MAC value, the *Coordinate Modal Assurance Criterion* (COMAC), which accounts for the spatial dependency of the degrees of freedom, is used by several authors to localise the damage (Allemang 2003, Parloo et al. 2003). These researches indicate that a level 2 damage identification based on (variants of) the MAC value is possible.

3.2 *Extended modal based identification methods*

The damage identification algorithm adopted in this and the earlier researches of the authors is the *modal strain energy damage index* (MSE-DI) algorithm. This method has not only been used by several other researchers, it has also appeared in a number of different variants. Modifications have been made to improve the performance and robustness of the algorithm. It lies beyond the scope of this article to address all variants that have appeared throughout the years, but the main characteristics of the algorithms are discussed for a thorough understanding of the algorithm in general. This understanding is essential to proceed to a quantitative severity estimation of the damage.

The base of the algorithm is found in the strain energy. The strain energy definition depends on the type of deformation. A distinction can be made between axial, bending and torsional deformations. The structure investigated in this research is a plate like structure, in which the bending deformations are the dominant deformations. Hence, the theory presented, is limited to the bending strain energy U, which for a beam reads

$$U = \frac{1}{2}\int_0^l \left[EI_y \left(\frac{\partial^2 u_z(x)}{\partial x^2} \right)^2 \right] \mathrm{d}x \tag{2}$$

with l the length of the beam EI_y the bending rigidity and $u_z(x)$ the displacement in z-direction as a function of the x-coordinate. A similar relation can be derived for a two-dimensional case

(plate) as was done by (Cornwell et al. 1999). This leads to more tedious equations, whereas the method itself does not change. Therefore only the one-dimensional case is explained.

It can be assumed that vibration of the structure is described sufficiently accurate in terms of a superposition of a number of modes N_{freq}, generally the modes of the lower natural frequencies: the system is considered to be linear. Secondly, the beam is discretised in N elements over the length of the beam. Hence, the contribution of each element of each of the participating mode shapes $u_z^{(n)}(x)$ to the total strain energy is proportional to

$$U_i^{(n)} = \frac{1}{2}\int_{z_{i-1}}^{z_i}\left[\left(EI_y\right)_i\left(\frac{\partial^2 u_z^{(n)}(x)}{\partial x^2}\right)^2\right]\mathrm{d}x$$
$$\text{with}: \quad U = \sum_{n=1}^{N_{freq}}\left(\alpha_n U^{(n)}\right) = \sum_{n=1}^{N_{freq}}\left(\alpha_n \sum_{i=1}^{N} U_i^{(n)}\right) \tag{3}$$

where the sub- or superscript n denotes the mode number, i the element number and α_n the modal participation factor. The definitions of the damage index start to deviate from this point. However, all are based on a comparison between the modal strain energy in the intact and damaged case – the latter indicated by tilde sign on top of the variable symbols. It is generally assumed that the total strain energy and total stiffness do not change significantly and that the damage is primarily located in a single element or a relatively low number of elements (Cornwell et al. 1999, Alvandi & Cremona 2006). As a result, the change in the ratio of the strain energy in a single element over the total strain energy is of interest.

Following the definition proposed in Cornwell et al. (1999), the ratio of fractional element stiffnesses of the damaged structure over the reference structure provides the base of the damage index:

$$\frac{\tilde{\gamma}_j^{(n)} \Big/ \tilde{\gamma}^{(n)}}{\gamma_j^{(n)} \Big/ \gamma^{(n)}} = \frac{\int_{x_{j-1}}^{x_j} \tilde{w}^{(n)}(x)\mathrm{d}x \Big/ \int_0^l \tilde{w}^{(n)}(x)\mathrm{d}x}{\int_{x_{j-1}}^{x_j} w^{(n)}(x)\mathrm{d}x \Big/ \int_0^l w^{(n)}(x)\mathrm{d}x} = \frac{\left(\int_{x_{j-1}}^{x_j} \tilde{w}^{(n)}(x)\mathrm{d}x\right)\left(\int_0^l w^{(n)}(x)\mathrm{d}x\right)}{\left(\int_{x_{j-1}}^{x_j} w^{(n)}(x)\mathrm{d}x\right)\left(\int_0^l \tilde{w}^{(n)}(x)\mathrm{d}x\right)} \tag{4}$$

where $w^{(n)}(x)$ represents the second term in the integrand of Equation 1 (the first term of the integrand, EI_y, is dropped as it is assumed to remain constant) and $\gamma_j^{(n)}$ the intregal of $w^{(n)}(x)$ over element j and $\gamma^{(n)}$ the intergral of $w^{(n)}(x)$ of the entire length l of the structure. This ratio is defined for each mode shape (superscript n). The information in each of the mode shapes is combined in the damage index β. There are several ways to achieve this, but in short it depends on how the modal information is summed. Cornwell et al. (1999), Hu & Wu (2009), Ooijevaar et al. (2010a, b) and Loendersloot et al. (2009, 2010) sum the numerator and denominator of the left-most term in Equation 4 separately, maintaining the fractional stiffnesses γ intact, whereas Choi et al. (2005a, b) suggest to sum the numerator and denominator of the right-most term in Equation 4 separately. Alvandi & Cremona (2006) first calculate the ratio, then sum over the number of modes involved and finally devided the index by the number of modes. The value of one is added to both the numerator and denominator in Equation 4 for either of the three versions of the summation by various authors (Stubbs et al. 1995, Farrar & Jauregui 1998a, b, Yang et al. 2004, Srinivasan & Kot 1998) to avoid the possible singularity in the index. It should be noted that this list of definitions and interpretations of the damage index β is far from complete. Other variants, partly discussed by the authors named as well, for example drop the assumption of a constant rigidity ($EI_y \neq \tilde{E}I_y$). However, it is beyond the scope of this article to discuss all variants. These are the main approaches, covering the majority of the implementations of the MSE-DI algorithm.

$$\beta_j = \frac{\sum_{n=1}^{N_{freq}} \left[\tilde{\gamma}_j^{(n)} \Big/ \tilde{\gamma}^{(n)} \right]}{\sum_{n=1}^{N_{freq}} \left[\gamma_j^{(n)} \Big/ \gamma^{(n)} \right]} \qquad \text{Cornwell et al. (1999)} \quad \text{Hu \& Wu (2009)} \quad \text{Ooijevaar et al. (2010a, b)} \quad \text{Loendersloot et al. (2009, 2010)} \qquad \text{(a)}$$

$$\beta_j = \frac{\sum_{n=1}^{N_{freq}} \left[\tilde{\gamma}_j^{(n)} \gamma^{(n)} \right]}{\sum_{n=1}^{N_{freq}} \left[\gamma_j^{(n)} \tilde{\gamma}^{(n)} \right]} \qquad \text{Choi et al. (2005a, b)} \qquad \text{(b)}$$

$$\beta_j = \frac{1}{N_{freq}} \sum_{n=1}^{N_{freq}} \left[\frac{\tilde{\gamma}_j^{(n)} \Big/ \tilde{\gamma}^{(n)}}{\gamma_j^{(n)} \Big/ \gamma^{(n)}} \right] \qquad \text{Alvandi \& Cremona (2006)} \qquad \text{(c)}$$

$$\beta_j = \frac{\sum_{n=1}^{N_{freq}} \left[\left(\tilde{\gamma}_j^{(n)} + \tilde{\gamma}^{(n)} \right) \Big/ \tilde{\gamma}^{(n)} \right]}{\sum_{n=1}^{N_{freq}} \left[\left(\gamma_j^{(n)} + \gamma^{(n)} \right) \Big/ \gamma^{(n)} \right]} \qquad \text{Srinivasan \& Kot (1998)} \qquad \text{(d)}$$

$$\beta_j = \frac{\sum_{n=1}^{N_{freq}} \left[\left(\tilde{\gamma}_j^{(n)} + \tilde{\gamma}^{(n)} \right) \gamma^{(n)} \right]}{\sum_{n=1}^{N_{freq}} \left[\left(\gamma_j^{(n)} + \gamma^{(n)} \right) \tilde{\gamma}^{(n)} \right]} \qquad \text{Stubbs et al. (1995)} \quad \text{Farrar \& Jauregui (1998a, b)} \qquad \text{(e)}$$

$$\beta_j = \frac{1}{N_{freq}} \sum_{n=1}^{N_{freq}} \left[\frac{\left(\tilde{\gamma}_j^{(n)} + \tilde{\gamma}^{(n)} \right) \Big/ \tilde{\gamma}^{(n)}}{\left(\gamma_j^{(n)} + \gamma^{(n)} \right) \Big/ \gamma^{(n)}} \right] \qquad \text{Yang et al. (2004)} \qquad \text{(f)} \qquad (5)$$

The summation, which ever way it is done, is an important and powerful aspect of the MSE-DI algorithm: it is not required to know a-priori which modes are most sensitive to damage. This is an important characteristic, since the location of the damage will affect which modes are most sensitive. The downside is that the modes that are not affected in a certain damage case dampen the value of the damage index β. This can cause a drop of the damage index below significance, resulting in a false negative damage notification (no notification, damage present). The set of modes must therefore be selected carefully in order to maintain sufficient sensitivity to damage while reducing the chance of undetected damages (see amongst others Choi et al. 2006).

The sensitivity of the parameter γ is relatively high, due to the fact that the curvature (second order derivate of the displacements) of the mode shapes is used. A small change in the mode shape, only resulting in a minimal change of the MAC value, can have a significant effect on the curvature (Pandey et al. 1991). However, it also implies that the mode shapes must be determined with a high accuracy to avoid erraneous results due to a poor representation of the mode shapes. This results in a relatively high number of measuring points for experimental cases (the number of nodes in numerical cases is generally not a bottleneck), whereas one of the objectives in the implementation of the MSE-DI algorithm also involves the reduction of the number of measuring points (Loendersloot 2009, Ooijevaar 2010a). It also implies that the method employed to calculate the derivatives of the mode shapes can affect the results.

It is worth noting that all formulations share a common characteristic: the participation of a mode in the actual vibration of the structure (the factor α in Equation 3) is dropped. Inherently, it is not possible to link the value of the damage index directly to damage severity in terms of

stiffness loss ratio (or something similar). The efforts done (Choi et al. 2006, Li et al. 2006) resulted in an underestimation of the damage severity.

Finally, the damage index β is generally normalised using the standard deviation σ and the mean μ of the damage index over all elements. This results in the value *Z*, defined in each element as:

$$Z_j = \frac{\beta_j - \mu}{\sigma} \tag{6}$$

Note that this normalisation is applied in the same way for all definitions of the damage index β, both strain energy and compliance based. The advantages are an increased value of the index at potential damage location and the possibility to directly assign a significance level.

3.3 *Implementation of the MSE-DI algorithm*

At this point, the mode shape curvatures are not yet discretised: γ is still formulated as an integral. In reality, these will be based on a set of measured data points or nodal displacements. One of the procedures to extract the mode shapes from the experimental data is to fit a cubic spline function through the responses measured at all (equidistant) points at the corresponding natural frequency (or close to it), as described by Ooijevaar et al. (2009). Similarly, a cubic spline function can be fit through a set of nodal displacements from the numerical model. Evidently, it is also possible to use the full set of nodal displacements. Problems may arise if the grid of nodal points is not equidistant. This will imply that the mode shape is described more accurately at line segments or areas with a higher nodal density. Consequently, the damage index will depend on the nodal density as well, which will make a severity estimation based on the damage index even more difficult.

Similarly, the height of the damage index depends on the cubic spline fit used, in particular the end conditions, but also the tolerance. Ooijevaar et al. (2009) discussed this matter briefly. A thorough discussion is beyond the scope of this paper, but it is important to acknowledge the effect of the fit parameters on the value of the damage index.

Once the spline functions are determined, the strain energy can be calculated by taking the second derivative of the spline functions. The second derivative is a stepwise linear function, since a cubic spline fit was employed. It was observed by Choi et al. (2008) that the higher order modes contribute disproportionally to the damage index. This is due to the higher curvatures in the higher modes. They suggest to use mass normalisation for the mode shapes but also to normalise the curvatures to level out the contribution of the modes. A highest value normalisation is used by Choi et al. (2008), although it is likely that a unit length normalisation will resort a similar effect. This is not further investigated. The need for a normalisation of the curvatures also depends on the definition of the damage index β (Equation 5): the formulation in Equation 5a is based on a fractional change of the mode shape curvature and hence the curvature is inherently normalised, whereas the curvatures are not inherently normalised in Equation 5b and 5c.

The final step to calculate the damage index is the integration of the strain energy. The curvatures are stepwise linear function, as stated, which makes the integrands $w^{(n)}(x)$ stepwise squared functions. The integration of these functions is straightforward, not only in the 1D case, but also in the 2D case. However, in general, the number of spline interpolation points is chosen higher than the number of measuring points (or the set of nodal displacements) and sufficiently high to use a linear numerical integration. The integral γ is therefore approximated by

$$\gamma_j^{(n)} \approx \frac{l}{2N}\left(\left(\frac{\partial^2 \hat{u}_y^{(n)}\left(x_j\right)}{\partial x^2}\right)^2 - \left(\frac{\partial^2 \hat{u}_y^{(n)}\left(x_{j-1}\right)}{\partial x^2}\right)^2\right) \tag{7}$$

The hat indicates it concerns the cubic spline representing the mass normalised mode shape. An alternative to the cubic spline fit is to use accurate mode shape predictions from numerical models, based on a dense grid of nodes. However, the results show that the match between numerically and experimentally determined mode shapes start to deviate at higher frequencies

(Loendersloot et al. 2010), which can result in a limitation of the frequency range that can be used, potentially reducing the sensitivity of the algorithm.

4 RESULTS & DISCUSSION

A numerical model was made in the commercial Finite Element package Abaqus®. A frequency analysis, to extract the natural frequencies and mode shapes, and a harmonic response analysis, to extract the frequency response functions, were subsequently executed. The frequency range for the harmonic response analysis was set equal to the frequency range of the measurements that were performed in parallel (Ooijevaar et al. 2011). The experimental results are used for validation of the FE model but are not discussed in this paper in detail.

The numerical analysis are ran for eleven different cases: the reference case and ten cases with an added mass of 10 to 100 grams (~0.25-2.5% of the total mass of the panel). Firstly, the natural frequencies and MAC-values are investigated. Secondly, the MSE-DI algorithm is applied to localise the added mass (structural change, or artificial 'damage') and finally an approach is discussed to estimate the added mass from the results, comparable to a damage severity estimation.

A measurement grid of 29 times 7 points was used (as was indicated in Figure 2). Nodes are defined at these exact locations and used to determine the mode shape. This method used to avoid parasitic weighting due to varying nodal densities. Moreover, it facilitates the comparison (and validation) with the experimental results. The final goal is to use the numerical model to improve the data analysis of experiments, in which case a denser grid of nodes can be used. That is beyond the scope of this article though.

4.1 *Natural frequencies and MAC-values*

The natural frequencies calculated by the numerical model, for all damage cases, and the experimental natural frequencies are listed in Table 2. Only the first 20 natural frequencies are listed. The reason is twofold: firstly, the modal density is high for the second half of the frequency range (90 modes were identified by the numerical model) and secondly it becomes difficult for the higher frequencies to match the experimental and numerical modes. The latter point is a combination of small descrepancies between the model and the experiment, measuring inaccuracies and the high modal density. It is questionable if sophisticated model updating technologies, that will help to increase the number of matching modes, will result in a better performance of the damage localisation algorithm and the severity estimation. The main reason is that one of the benefits of the MSE-DI algorithm is said to be that only a limited number of modes need to be included (Stubs et al. 1995). However, for severity estimation it may be relevant to improve the match between the numerical model and the experimental results.

The change of the natural frequencies due to the added mass varies per mode, but is relatively small. In general, it is smaller than the difference currently observed between the numerical model and the experiments.

The MAC-values between the intact (no added mass) numerical and experimental modes are shown in Figure 3. It is clear that a sufficient correspondence between model and experiment is found for the first 10-15 modes (MAC>0.8), although some of these modes show a somewhat lower MAC value. The exact cause of the mismatch is difficult to retrieve, as the number of potential sources is large. The main reasons are most likely differences in the (local) material properties, such as deviations from the intended fibre angle in the different layers and small variations in the thickness of each layer, resulting in different mechanical properties. Another source is the mounting in the experiments: the panel is attached to two rubber straps, with a relatively low stiffness. This complicates a correct representation of the boundary conditions. Finally, the accuracy of the measurement will affect the match of higher modes.

Table 2. Natural frequencies of the numerical model for the reference case (no added mass) and the 10 cases with added mass. The right-most column contains the experimentally determined frequencies.

	frequency [Hz]										
		added mass [g]									
mode	ref	10	20	30	40	50	60	70	80	90	100	exp
1	19.75	19.74	19.73	19.72	19.70	19.69	19.68	19.67	19.66	19.65	19.64	-
2	80.72	80.69	80.65	80.61	80.58	80.54	80.50	80.46	80.43	80.39	80.35	89.07
3	94.07	94.00	93.93	93.86	93.78	93.71	93.64	93.57	93.50	93.43	93.35	102.54
4	102.08	102.08	102.08	102.08	102.08	102.08	102.08	102.08	102.08	102.08	102.08	108.23
5	119.51	119.50	119.49	119.49	119.48	119.47	119.46	119.45	119.44	119.43	119.42	132.83
6	155.11	155.02	154.92	154.81	154.68	154.53	154.36	154.17	153.94	153.68	153.39	161.53
7	165.88	165.53	165.16	164.76	164.33	163.88	163.42	162.94	162.46	161.99	161.53	178.42
8	169.82	169.70	169.60	169.51	169.43	169.36	169.30	169.25	169.20	169.16	169.13	183.10
9	170.87	170.86	170.86	170.85	170.85	170.85	170.84	170.84	170.84	170.84	170.84	196.73
10	200.84	200.70	200.55	200.39	200.21	200.02	199.82	199.60	199.36	199.10	198.82	216.85
11	220.47	220.46	220.45	220.44	220.42	220.39	220.36	220.32	220.26	220.17	220.02	229.81
12	235.65	234.76	233.78	232.73	231.60	230.40	229.14	227.84	226.52	225.21	223.95	250.91
13	239.28	239.28	239.27	239.27	239.27	239.27	239.27	239.27	239.27	239.27	239.27	256.87
14	264.74	264.61	264.47	264.30	264.11	263.89	263.63	263.34	263.00	262.61	262.17	-
15	287.52	286.40	285.13	283.75	282.27	280.74	279.19	277.68	276.25	274.93	273.74	300.50
16	293.71	293.68	293.66	293.64	293.62	293.60	293.59	293.57	293.56	293.55	293.54	315.21
17	298.26	297.98	297.73	297.51	297.31	297.14	296.99	296.86	296.74	296.64	296.55	324.86
18	306.56	306.51	306.47	306.43	306.40	306.37	306.33	306.30	306.28	306.25	306.23	348.80
19	346.04	345.52	344.89	344.15	343.26	342.22	341.01	339.64	338.15	336.59	335.01	360.97
20	367.46	366.83	366.11	365.28	364.35	363.32	362.22	361.09	359.99	358.96	358.04	377.43

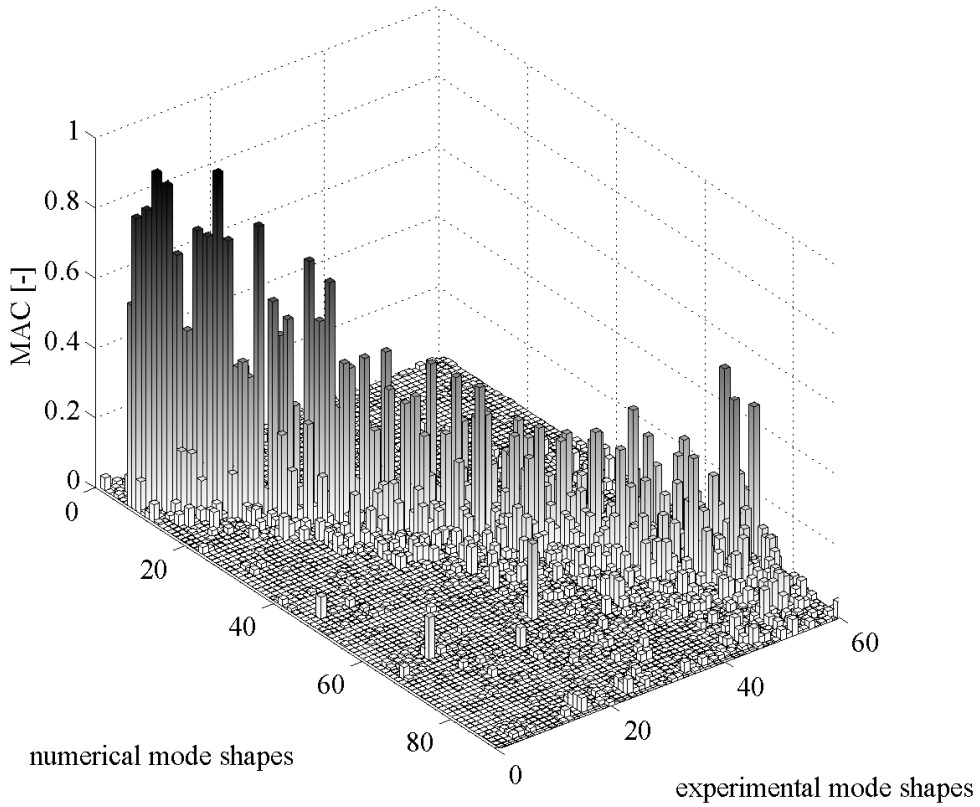

Figure 3. MAC values of the experimental mode shapes versus the numerical mode shapes (no added mass). The first numerical modes are not measured as they are below the lower limit of the frequency range of the measurements. The first 10 to 15 modes fit reasonably.

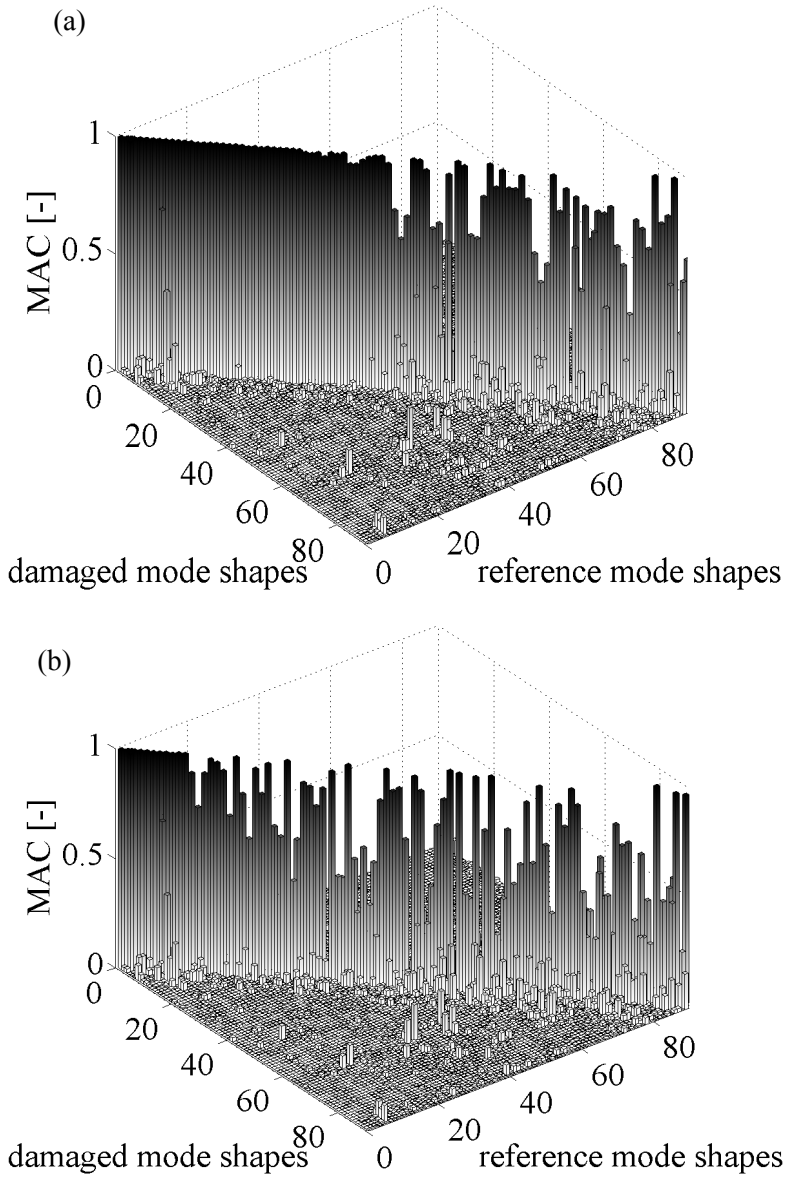

Figure 4. MAC values for the numerical cases with (a) an added mass of 10 grams and (b) an added mass of 100 grams.

A significant change of the MAC values is observed comparing the (numerical) cases with the added mass (Fig. 4). Two cases are shown: an added mass of 10 grams and of 100 grams. The change in MAC values clearly indicates that there has occurred a change in the structure, where the amount of change is an qualitative indication of the amount of added mass. However, the change in MAC-values does not provide any information of the location of the damage. Still, the MAC-value is useful for the localisation. The damage identification based on the modal strain energy relies on changes in mode shape curvatures and therefore – on could say – magnifies subtle changes in the MAC-value. However, a very low MAC-value implies that the modes do not match at all and as a consequency the curvatures will differ significantly over the entire mode shape, rather than only in the neighbourhood of the damage. This can lead to a number of erroneous peaks in the damage index (or 'noise'), potentially even to false positives (indication of damage at a location where no damage is present). To this end, the number of modes that participate in the MSE-DI algorithm is limited to those modes that have a MAC-value between 0.5 and 1.0. It could be argued to chose a more narrow range, in particular excluding modes that have not changed due to the damage (MAC=1). A number of tests revealed

that the effect is limited and that the range suggested here, provides the best results. However, it should be recognised that this is not valid in general.

4.2 *MSE-DI: localisation of the damage*

A 1D MSE-DI algorithm is applied using cubic spline fit mode shapes of 128 data points over the length of the panel. This results in seven data sets of the damage index β (or Z in normalised form) over the width of the panel (Fig. 2, first data set is based on P1-P29, the 7th on P175-P203). The reason to use a 1D algorithm at this point is the observation that the sensitivity of the damage index algorithm in the direction of the lower stiffness is significantly lower than the sensitivity in the stiffer direction of the panel – which corresponds to the direction of the stiffeners (Loendersloot et al. 2010, Ooijevaar 2010b). However, this limits the localisation abilities in the width direction.

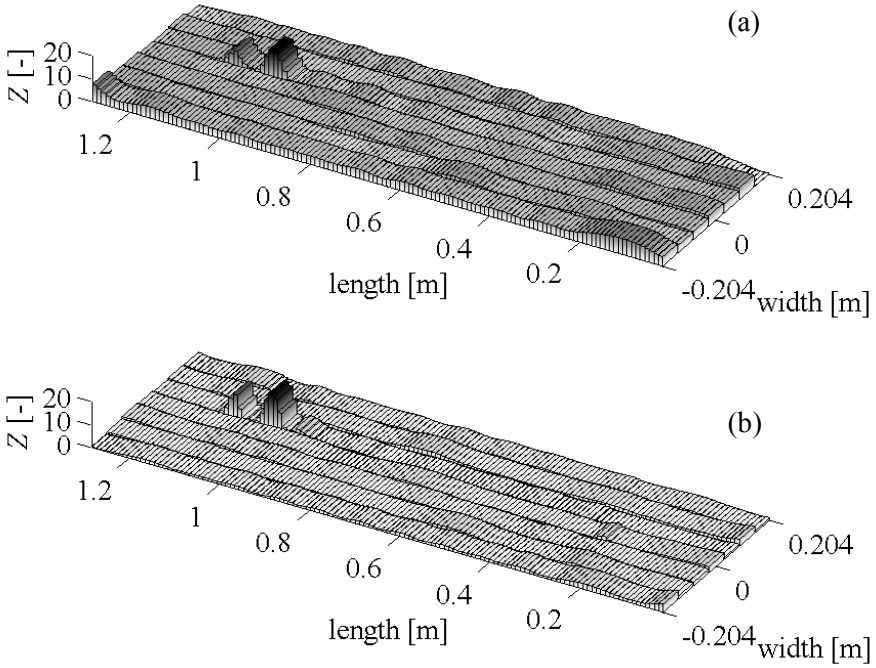

Figure 5. Normalised damage index Z for (a) an added mass of 10 grams and (b) an added mass of 100 grams.

The normalised damage index Z for the different damage cases is shown in Figure 5. A clear peak indicates the location of the damage. For all cases, the location of the damage is predicted to be approximately at $(x,y)=(1.025,0.068)$. The exact location of the added mass is $(x,y)=(1.03,0.08)$, resulting in a relative deviation of 0.5% in the length direction and 15% in the width direction. The high deviation in the width direction is evidently caused by the use of a 1D algorithm in length direction only. A 2D algorithm is required to improve the accuracy.

However, a secundary peak is also present. This is either a false positive (indication of damage, but no actual change in the structure) or a secundary effect of the added mass, caused by the set of modes included in the algorithm. The latter is assumed to be the most likely explanation, given the height of the peak and the consistency in the location.

It is also observed that the maximum reaches approximately the same value, irrespective of the amount of added mass. This is visualised in Figure 6, which shows the maximum value of all peaks that were found as a function of the relative amount of added mass (compared to the total mass of the panel). A distinct convergence is present. Another observation is that the number of false peaks increases with increasing mass. This implies that the mode shapes are affected at more locations than only at the region of the added mass. The secundary peaks remain significantly lower than the maximum peaks, but to raise above the significance level (which is generally 2 or 3 depending on the confidence desired). This situation could be comparable to a

situation with two (or more) added masses, where one added mass is significantly higher than the other(s). Also here, a 2D implementation may help to distinguish false negatives from true positives.

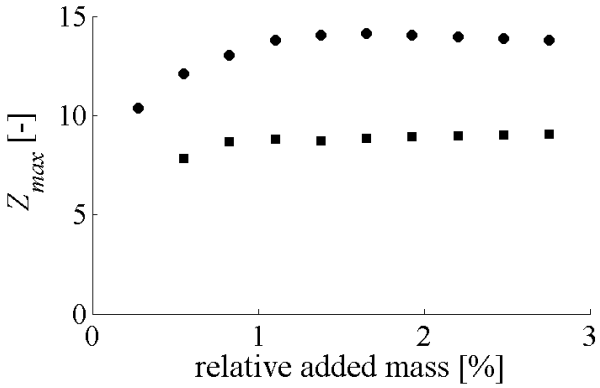

Figure 6. Maximum value for the normalised damage index Z as a function of the relative amount of added mass. The circles indicate the first peak, the squares the secundary peak.

Possibly the most important conclusion that can be drawn from Figure 6 is that there is no useful relation between the added mass and the value of the damage index. This is a direct consequence of the participation factor α being dropped out of Equation 3. The advantage of the damage index Z is an improved detectability and – in the numerical case – that only a frequency analysis suffices to determine the location of the damage, but the price is the inability to estimate the extent of the damage accurately.

4.3 *Damage severity estimation*

A logical step to proceed to an estimation of the damage is to combine the results of the direct and extended modal based algorithms. At this point, the location of the damage is known (with a certain accuracy) as well as the frequency response of the intact and damaged structure. The participation of each of the modes is still – implicitly – present in the frequency response function. As a result, it contains absolute values for the amplitudes and therefore has the potential to serve as source for a more accurate severity estimation.

The most apparent change in the frequency response function is the shift of the natural frequencies of some of the modes. An estimation of the amount of added mass (here representing the damage) requires a relation between the shift of the natural frequencies and the added mass. This relation is found by analysing the principle of generalised mass. The generalised mass matrix M_r is defined as:

$$M_r = \Phi_r^T M \Phi_r \tag{8}$$

with M the mass matrix and Φ_r the normalised mode shapes (normalised on the maximum displacement). The generalised mass matrix is a diagonal lumped mass matrix that is typically unknown. It can be derived by adding small masses to the structure (Dillinger et al. 2005). The generalised mass $m_r^{(n)}$ of a certain mode n (the n^{th} diagonal term of M_r) can be written as

$$m_r^{(n)} = \frac{\left(\tilde{f}^{(n)}\right)^2}{\left(f^{(n)}\right)^2 - \left(\tilde{f}^{(n)}\right)^2} \sum_{j=1}^{N} \left[\Delta m_j x_j^{(n)}\right] \approx -\frac{f^{(n)}}{2\Delta f^{(n)}} \sum_{j=1}^{N} \left[\Delta m_j x_j^{(n)}\right] \tag{9}$$

with $f^{(n)}$ the n^{th} natural frequency (tilde refers to damaged case), Δm_j the j^{th} of a total of N added masses, $\Delta f^{(n)}$ the frequency shift and $x_j^{(n)}$ the normalised displacement at the location of the j^{th} added mass of the n^{th} mode. The last step is achieved by ignoring the higher order terms when expanding the fraction and writing the frequency of the damage in terms of a variation on the reference frequency:

$$\tilde{f}^{(n)} = f^{(n)} + \Delta f^{(n)} \tag{10}$$

Note that this analysis requires knowledge of the location of the added mass $x_j^{(n)}$. This is obtained from using the MSE-DI algorithm. Analysing the structure for a range of added masses allows to establish the relation between the shift of the natural frequency and the amount of mass added to the structure. In this case N=1, for which case the relation between the frequency shift and added mass reads

$$\Delta m = -\frac{2m_r^{(n)}}{f^{(n)}\left(x^{(n)}\right)^2}\Delta f \tag{11}$$

Note that $x^{(n)}$ refers to displacements at the exact location of the added mass, whereas the algorithm provides an approximation of this location. Moreover, the peak in the normalised damage index Z is associated with four data points (corners of the ground surface of each bar in Figure 5). The relation in Equation 11 is depicted in Figure 7 for a number of modes, which were matched based on a minimum MAC value of 0.85 (between numerical modes). The dashed line is based on calculated frequencies shift (by the numerical model) and known added masses.

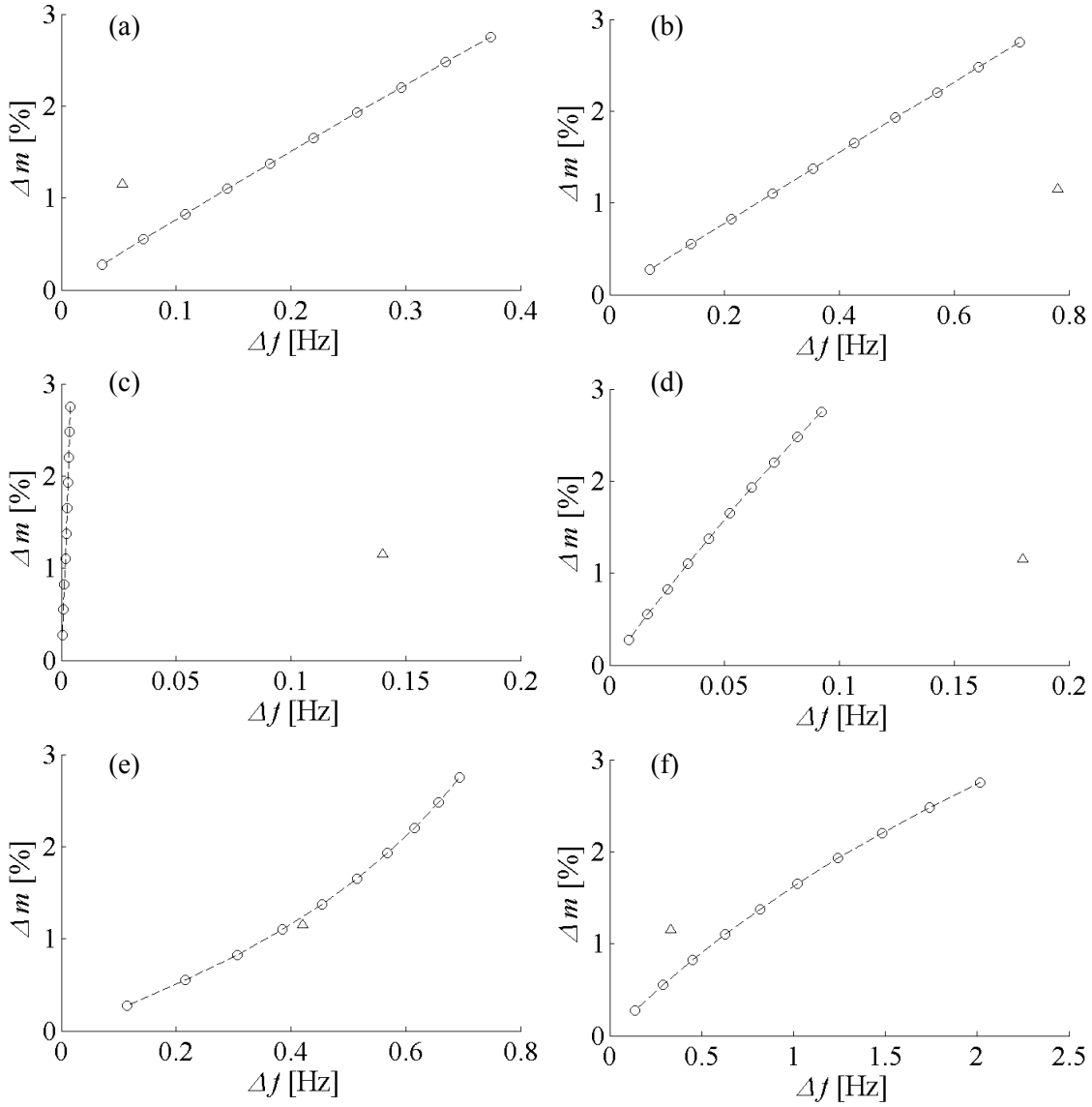

Figure 7. Relative mass change versus frequency shift for 6 cases. The circles are the numerical results with 10 to 100 grams of added mass, whereas the triangle are based on the measured data. (a) mode 8, (b) mode 9, (c) mode 10, (d) mode 11, (e) mode 14 and (f) mode 16.

It can be observed that the relation appears to be linear in most cases. This is expected if the change of the mode shape is only limited. Both the generalised mass $m_r^{(n)}$ and the frequency $f^{(n)}$ are related to the reference situation. This method is employed to determine the generalised mass matrix more or less based on the concept of linear perturbation: it is assumed that the added masses does not affect the response $x^{(n)}$, which is not necessarily the case here.

The triangles in Figure 7 indicate the experimentally determined frequency shift (Ooijevaar et al. 2011) for the given added mass of 42 grams. The descrepancy between the dashed line, derived from the numerical simulation, and the experimental results can be explained by the differences in the model and the experiments: a difference of approximately 5-10% in natural frequencies is observed, as can be concluded from Table 2. However, the relation between the shift in the frequency and the added mass depends on the generalised masses $m_r^{(n)}$ and frequencies $f^{(n)}$ of the reference state and on the response of the point $x^{(n)}$ of the damaged case. For the first two parameters, accurate models can be developed, for example using model updating techniques and/or a comprehensive experimental program. This only needs to be done once. The last parameter is obtained accurately employing a damage localisation method such as the MSE-DI algorithm discussed here.

So far, the 'damage' was represented by an added mass. Normally, damage will be reflected in a decrease of the stiffness. Hence, a similar procedure must be followed based on the generalised stiffness K_r, defined in analogy with Equation 8 as

$$K_r = \Phi_r^T K \Phi_r \tag{12}$$

It is expected that a shift in the natural frequencies will occur as a result since the generalised natural frequencies ω_r (in radians) are defined as:

$$\omega_r = \sqrt{\frac{K_r}{M_r}} \tag{13}$$

However, the result of measurements on panels before and after a 10-50J impact load (Ooijevaar et al. 2010b, Ooijevaar et al. 2011) indicate lower shifts of the natural frequencies. As a result, the step from damage severity estimation of a change in the structure by adding a small mass to that of a change in the stiffness of the structure needs further experimental and numerical investigation.

5 CONCLUSIONS & RECOMMENDATIONS

The work presented here, reflects the difficulties encountered in damage severity estimations. One of the conclusions that can be drawn is that the road from level 1 to level 3 and even 4 or 5 can not be taken with a single method. Specific methods were developed to enhance the identification of the damage, leading to more accurate predictions of the location of the damage and the size of the damage (level 2). However, the algorithms involved do not allow for a quantitative estimation of the damage severity, due to the fact that the damage index is merely a mathematical rather than a physical quantity.

This first conclusion certainly does not judge the extended modal based damage identification algorithms developed, that are based on derived modal parameters such as the modal strain energy. It remains true that these algorithms are significantly more powerful in detection and localisation of damage than algorithms that are confined to direct modal parameter, such as the natural frequencies, mode shapes and MAC values. In conjunction however, the two families of algorithms offer the potential to proceed to the next level of damage identification.

Moreover, this work stresses the fact that a damage identification algorithm is an algorithm that has to be developed for each specific application. The performance of the identification algorithms can be significantly different for other applications, turning around the observations and the resulting conclusions on a certain algorithm: it is made-to-measure work.

The method of combining localisation methods with the theory of generalised mass is shown to relate frequency shifts with the change of the structure in a quantitative manner. Certainly, the numerical model must be matched with the experimental results, more than is necessary to

acquire an accurate prediction of the location of the change in the structure (either damage or added mass). In this, some work is still ahead to match the numerical model with the experimental results more accurately.

Moreover, future investigation is required to adapt the method proposed for a change in stiffness rather than a change in mass. Theory indicates the possibilities, but experimental results have already indicated that this is a challenging task.

Another important observation is that the data used for localisation of damage in real applications can also be used for the severity estimation: generally, the modal parameters, such as natural frequencies and damping can be extracted from the response analysis performed (which can be either EMA or OMA based). Hence, no additional measurements are required. Numerical models need to be extended to obtain the same information, but this can be achieved at low computational costs.

A number of other unresolved issues are related to the specific material used in this research: composites. The location and to a certain extent the severity of the damage can be obtained, but there is no link yet with the type of damage, which is equally important for a good esimation of the damage severity

6 ACKNOWLEDGEMENTS

The authors kindly acknowledge Fokker Aerostructures for manufacturing the composite panels on which the experiments were performed. This work is carried out in the framework of the Eurpean project Clean-Sky Eco Design (grant number CSJU-GAM-ED-2008-001).

REFERENCES

Allemang R. (2003), The modal assurance criterion – twenty years of use and abuse, *Sound and Vibration*, 1:14-21

Alvandi A.A. and Cremona C.B. (2006), Assessment of vibration based damage identification techniques, *Journal of Sound and Vibration*, 292(1-2):179-202

Choi S., Park S. and Stubbs N. (2005a), Nondestructive damage detection in structures using changes in compliance, *International Journal of Solids and Structures*, 42:4494-4513

Choi S., Park S., Yoon S. and Stubbs N. (2005b), Nondestructive damage identification in plate structures using changes in modal compliance, *NDT&E International*, 38:529-540

Choi S., Park S., Park N.-H. and Stubbs N. (2006), Improved fault quantification for a plate structure, *Journal of Sound and Vibration*, 297:865-879

Choi F.C., Li J., Samali B. and Crews K. (2008), Application of the modified damage index method to timber beams, *Engineering Structures*, 30:1124-1145

Cornwell P., Doebling S.W., Farrar C.R. (1999), Application of the strain energy damage detection method to plate-like structures, *Journal of Sound and Vibration*, 224(2):359-374

Dillinger S., Mühlbauer K., Gambietz W. and Gautier F. (2005), Determination of the generalized mass from vibration test data by adding mass, *IMAC-XXIII: Conference & Exposition on Structural Dynamics*, Orlando, Florida, USA

Fan W. and Qiao P. (2011), Vibration based damage identification methods: A review and comparative study, *Structural Health Monitoring*, 10(1):88-111

Farrar C.R. and Jauregui D.A. (1998a), Comparative study of damage identification algorithms applied to a bridge: I experiments, *Smart Materials and Structures*, 7(5):704-719

Farrar C.R. and Jauregui D.A. (1998b), Comparative study of damage identification algorithms applied to a bridge: II numerical study, *Smart Materials and Structures*, 7(5):720-731

Fritzen C.-P. and Kraemer P. (2009), Self-diagnosis of smart structures based on dynamical properties, *Mechanical Systems and Signal Processing*, 23:1830-1845

Grouve W.J.B., Warnet L., Boer A. de, Akkerman R. and Vlekken J. (2008), Delamination detection with fibre bragg gratings based on dynamic behaviour, *Composite Science and Technology*, 68:2418-2424

Hu H. and Wu C. (2009), Development of scanning damage index for the damage detection of plate structures using modal strain energy method, *Mechanical Systems and Signal Processing*, 23(2):274-287

Ihn J. and Chang F. (2008), Pitch-catch active sensing methods in structural health monitoring for aircraft structures, *Structural Health Monitoring*, 7(1):5-19

Kudela P., Krawczuk M. and Ostachowicz W. (2007), Wave propagation modelling in 1D structures using spectral finite element, *Journal of Sound and Vibration*, 300(1-2):88-100

Kudela P., Ostachowicz W. and Zak A. (2008), Damage detection in composite plates with embedded PZT transducers, *Mechanical Systems and Signal Processing*, 22(6):1327-1335

Kudela P. and Ostachowicz W. (2009), A multilayer delaminated composite beam and plate elements: reflections of lamb waves at delamination, *Mechanics of Advanced Materials and Structures*, 16(3):174-187

Lee B. and Staszewski W. (2003a), Modelling of Lamb waves for damage detection in metallic structures: Part I. Wave propagation, *Smart Materials and Structures*, 12(5):804-814

Lee B. and Staszewski W. (2003a), Modelling of Lamb waves for damage detection in metallic structures: Part II. Wave interactions with damage, *Smart Materials and Structures*, 12(5):815-824

Lee J.J. and Yun C.B. (2006), Damage diagnostics of steel girder bridges using ambient vibration data, *Engineering Structures*, 28:912-925

Li H., Fang H. and Hu S.-L. J. (2007), Damage localization and severity estimation for three-dimensional frame structures, *Journal of Sound and Vibration*, 301:481-494

Loendersloot R., Ooijevaar T.H., Warnet L., Akkerman R. and Boer A. de (2009), Vibration Based Structural Health Monitoring in Fibre Reinforced Composites Employing the Modal Strain Energy Method, in *Proceedings of the International Conference Integrity Failure and Reliability*, 16 pages

Loendersloot R., Ooijevaar T.H., Warnet L., Boer A. de and Akkerman R. (2010), Vibration based structural health monitoring of a composite plate with stiffeners. In: *International Conference on Noise and Vibration Engineering*, ISMA 2010, Leuven

Montalvão D., Maia N.M.M. and Ribeiro A.M.R. (2006), A review of vibration-based structural health monitoring with special emphasis on composite materials, *The Shock and Vibration Digest*, 38(4):295-326

Ndambi J.-M., Vantomme J. and Harri K. (2002), *Damage assessment in reinforced concrete beams using eigenfrequencies and mode shape derivatives*, Engineering Structures, 24:501-515

Ooijevaar T.H., Loendersloot R., Warnet L.L., Boer A. de and Akkerman R. (2010a), Vibration based Structural Health Monitoring of a composite T-beam, *Composite Structures*, 92(9):2007-2015

Ooijevaar T.H., Loendersloot R., Warnet L.L., Boer A. de and Akkerman R. (2010b), Vibration based structural health monitoring of a composite plate structure with multiple stiffeners. In *Proceedings of the European Workshop on Structural Health Monitoring*

Ooijevaar T.H., Loendersloot R., Warnet L.L., Boer A. de and Akkerman R. (2011), Structural health monitoring of an advanced composite aircraft structure using a modal based approach, submitted and accepted for oral presentation at IWSHM-8, Stanford, USA

Pandey A.K., Biswas M., Samman M.M. (1991), Damage detection from changes in cuvature mode shapes, *Journal of Sound and Vibration*, 252(2):223-238

Parloo E., Guillaume P. and Overmeire M. van (2003) Damage assessment using mode shape sensitivities, *Mechanical Systems and Signal Processing*, 17(3):499-518

Raghavan A. and Cesnik C. (2007), Review of guided-wave structural health monitoring, *The Shcok and Vibration Digest*, 39(2):91-114

Salawu O.S. (1997), Detection of structural damage through changes in frequency: a review, *Engineering Structures*, 19(9):718-723

Schulte R.T. and Fritzen C.-P. (2010), Modelling of Wave-Based SHM Systems Using the Spectral Element Method, *Proceedings in Applied Mathematics and Mechanics*, 10:15-18

Schwarz J.B. and Richardson M.H. (1999) *Experimental Modal Analysis*, Vibrant Technology Inc.

Srivnivasan M. and Kot C. (2004), Damage index algorithm for a circular cylindrical shell, *Journal of Sound and Vibration*, 215(3):587-591

Staszewski W., Mahzan S. and Traynor R. (2009), Health monitoring of aerospace composite structures – active and passive approach, *Composites Science and Technology*, 69(11-12):1678-1685

Stubbs N., Kim J.T. and Farrar C.R. (1995), Field verification of a nondestructive danage localization and severity estimation algorithm, In *Proceedings of the 13th International Modal Analysis Conference*, pages 210-218

Stubbs N., Park S., Sikorsky C. and Choi S. (2000), A global non-destructive damage assessment methodology for civil structures, *International Journal of Systems Science*, 31(11)1361-1373

Su Z., Ye L. and Lu Y., Guided Lamb waves for identification of damage in composite structures: a review, *Journal of Sound and Vibration*, 295(3-5):753-780

Yang H., Li H. and Hu S. (2004), Damage localization for offshore structures by modal strain energy decomposition method, *Proceedings of the Americal Control Conference*, 4207-4212